

Supporting Information for Ultrafast Charge Transfer at a Quantum Dot/2D Materials Interface Probed by Second Harmonic Generation

Aaron J. Goodman,[†] Nabeel S. Dahod,[‡] and William A. Tisdale^{*,‡}

[†]*Department of Chemistry, Massachusetts Institute of Technology*

[‡]*Department of Chemical Engineering, Massachusetts Institute of Technology*

E-mail: tisdale@mit.edu

Supporting Information

Transient SHG Response of a Bare WS₂ Monolayer

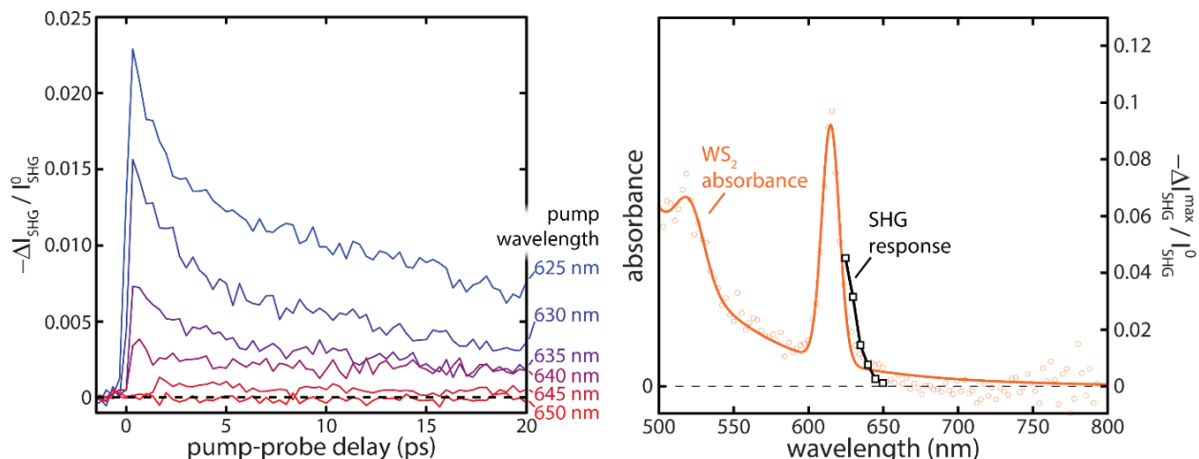


Figure 1: *left*: Transient SHG response of bare WS₂ monolayer. The colored traces represent experiments performed with different excitation wavelengths as indicated. The fluence is kept constant. *Right*: The maximum transient SHG response for a given excitation wavelength (black line) is plotted on the same graph as the bare WS₂ absorbance spectrum (open circles, orange line: smoothed guide to the eye). The magnitude of the transient SHG response closely follows the WS₂ absorption spectrum.

To show that the transient SHG signals observed in the main text arose from absorption by the CdSe dots – and not by direct photoexcitation of the WS₂ layer – we performed time-resolved SHG microscopy on a bare WS₂ monolayer. Though the monolayer shows appreciable transient response when excited by $\lambda = 625, 630, 635, 640,$ and 645 nm pump pulses, it shows no discernible response when excited with the excitation spectrum used in the main text ($\lambda = 650$ nm). The transient signals for QDs-on-WS₂ presented in the main text reached maxima of roughly $-\frac{\Delta I_{\text{SHG}}}{I_0^{\text{SHG}}} \approx 0.01 - 0.02$ at 650 nm excitation wavelength, which is more than an order of magnitude larger than the transient SHG response of the bare WS₂ at the same excitation wavelength.

QD Film Absorbance

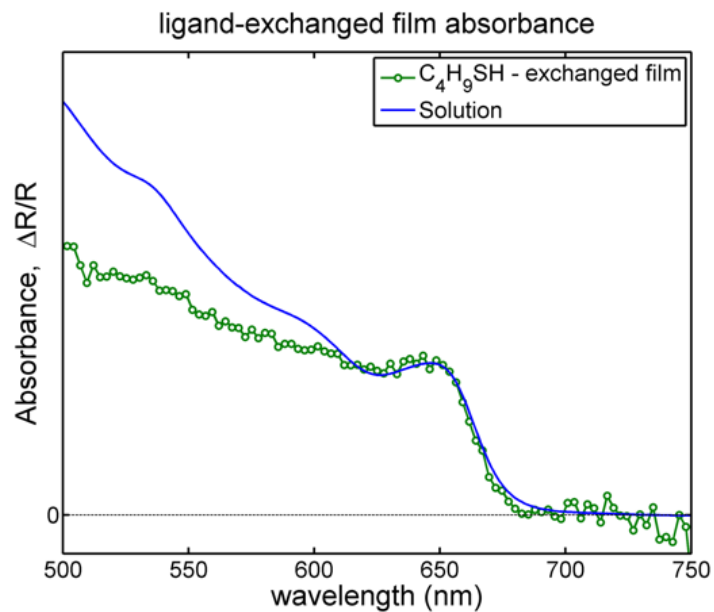


Figure 2: The QD solution absorbance spectrum presented in the main text is plotted (blue line) with the QD film reflectivity spectrum ($\Delta R/R$) after butane-thiol ligand exchange. The ground state absorption spectrum is not changed near the excitation resonance following ligand exchange.

Pump-Probe SFG Cross Correlation

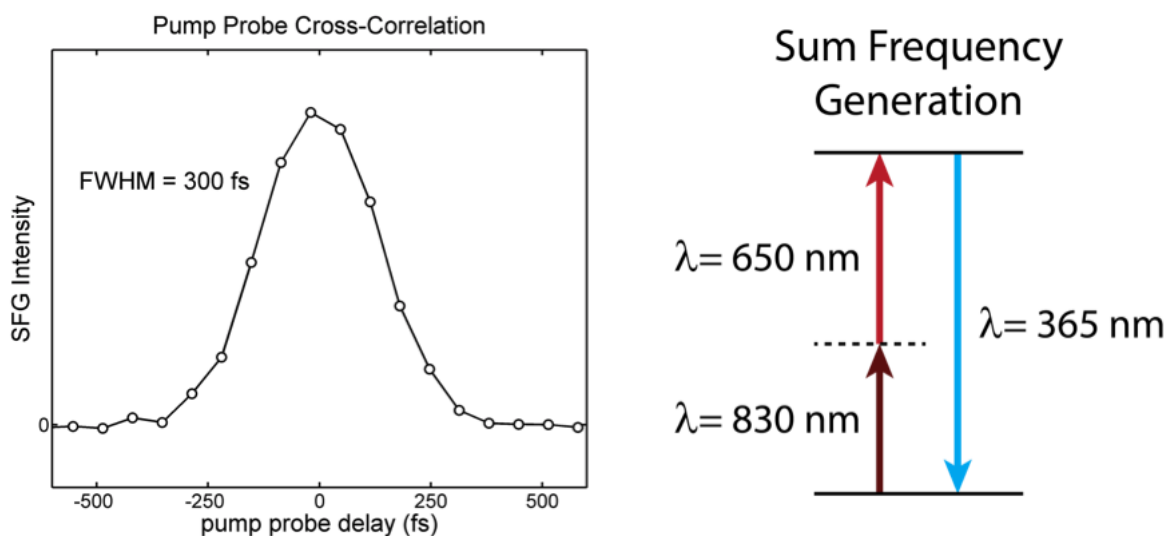


Figure 3: *Time resolution of the SHG microscope.* Sum frequency generation (SFG) was performed by mixing the pump and probe pulses in monolayer WS_2 . The SFG signal was filtered by a short pass filter to remove the pump, probe, and the probe second harmonic, and detected with the same PMT used in time-resolved SHG experiments. The SFG cross correlation represents the convolution of the pump and probe intensity profiles.

Octanethiol and Dodecanethiol Traces

As mentioned in the main text, oscillatory components were never observed in the octanethiol- and dodecanethiol-capped samples. These samples generally had smaller signals due to the weaker electronic coupling (charge transfer was less likely), but data collected with the same acquisition time and fluences never exhibited the oscillations seen in the ethanethiol- and butanethiol-capped samples. Exemplar traces for the long-ligand samples are plotted below for comparison.

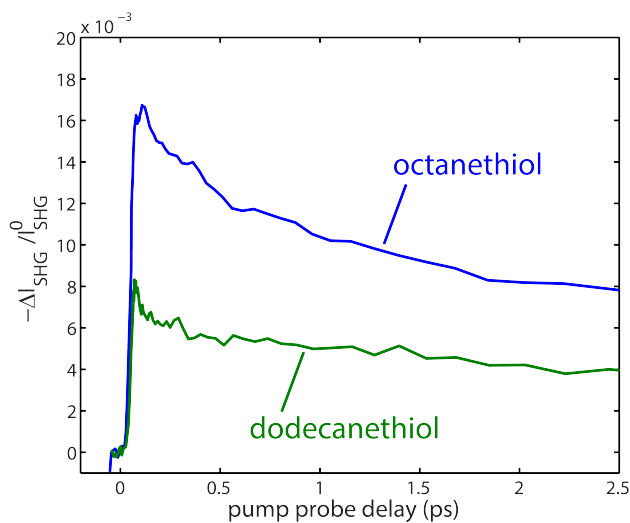


Figure 4: Example data collected from samples coated with octanethiol- (blue) and dodecanethiol- (green) capped dots. Though the data were collected for the same length of time as the data in Fig. ?? in the main text, oscillations were never observed in these samples.

Transient Curve Fitting

Curves were fit as the solutions to a system of coupled differential equations reflecting the rate diagram depicted in Fig. 5. This model assumes that the SHG signal probes donated free carriers in the WS₂ conduction band ($[WS_2^{*,hot}] + [WS_2^*]$ in Fig. 5). Apart from the system ground state, the model considers three excited states: The excited QD [QD*], a hot transferred electron in the WS₂ conduction band $[WS_2^{*,hot}]$ and a cooled transferred electron in the WS₂ conduction band $[WS_2^*]$. The excited QD is coupled to the ground state with some decay rate constant k_{decay} and to the WS₂ conduction band with the electron transfer rate constant k_{ET} . The model assumes electron transfer is symmetric ($k_{ET} = k_{BET}$). The hot electron in the WS₂ conduction band is coupled to the ground state via the rate constant k_{diff1} and to the cooled state via the constant k_{cool} . Cooled charges in the WS₂ conduction band can find holes with which to combine with rate constant k_{diff2} . These three states coupled by the relevant rate constants naturally lead to a set of coupled differential equations:

$$\frac{d[QD^*]}{dt} = -k_{ET}[QD^*] - k_{decay}[QD^*] \quad (1)$$

$$\frac{d[WS_2^{*,hot}]}{dt} = k_{ET}[QD^*] - k_{cool}[WS_2^{*,hot}] - k_{diff1}[WS_2^{*,hot}] \quad (2)$$

$$\frac{d[WS_2^*]}{dt} = k_{cool}[WS_2^{*,hot}] - k_{diff2}[WS_2^*]. \quad (3)$$

To model the impulsive excitation of the QD film in the experiment, these differential equations were initialized with the initial condition ($[QD^*] = N_0$, $[WS_2^{*,hot}] = 0$, $[WS_2^*] = 0$) and solved numerically. The charged WS₂ states were summed and convolved with the experimentally measured IRF for direct comparison with data. The rate constants coupling the three states were then found to minimize the sum of the squared residuals between the generated curve and the experimental data.

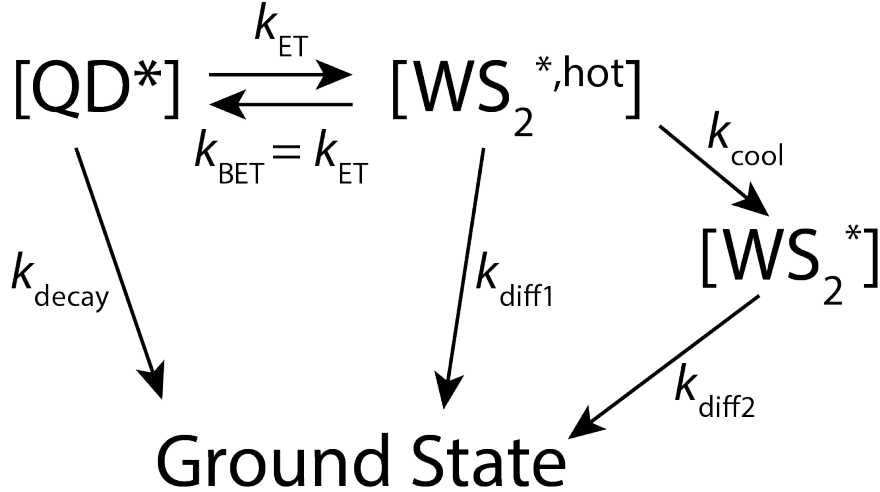


Figure 5: Rate diagram depicting the excited state processes available to a photoexcited electron. Upon excitation, the electron resides on the donor QD. From there, it can decay to the ground state directly or transfer to a hot WS_2 excited state. From there it can back transfer, return to the QD ground state directly, or relax to the WS_2 band edge. Once cooled, the electron in WS_2 eventually finds a hole with which to combine returning the system to the ground state.

Resolvable Electron Transfer Time Constants

The cross correlation between the pump and probe pulse was 300 fs wide), which is a good starting point when determining the minimum electron transfer time resolvable with our instrument. In our experiment, the electron transfer time is reflected in the transient SHG signal rise time whose width has two contributions: broadening due to the finite duration of the pump and probe pulse as well as broadening due to stochastic electron transfer with rate constant k_{ET} . It is much easier to resolve transfer times that are comparable to the pump-probe cross correlation width, but with adequate signal-to-noise it is still possible to resolve electron transfer times that are substantially shorter. With the curve fitting described above, the shortest resolvable electron transfer time is determined by the signal-to-noise ratio for the experimental data. This concept is illustrated in Fig. 6 where we plot the transient SHG signal for ethane-thiol coated dots on WS_2 in green. The electron transfer time for this data is not resolvable by our measurement and the rise time represents the width of

the IRF (plotted in red). Blue lines represent fits to the data in green with altered input values for the electron transfer rate constant k_{ET} . By eye, the generated curves begin to deviate from the experimental data when k_{ET} is between 40 and 50 fs. For this reason, 50 fs is the minimum electron transfer time discernible with the signal-to-noise ratio achieved in our data.

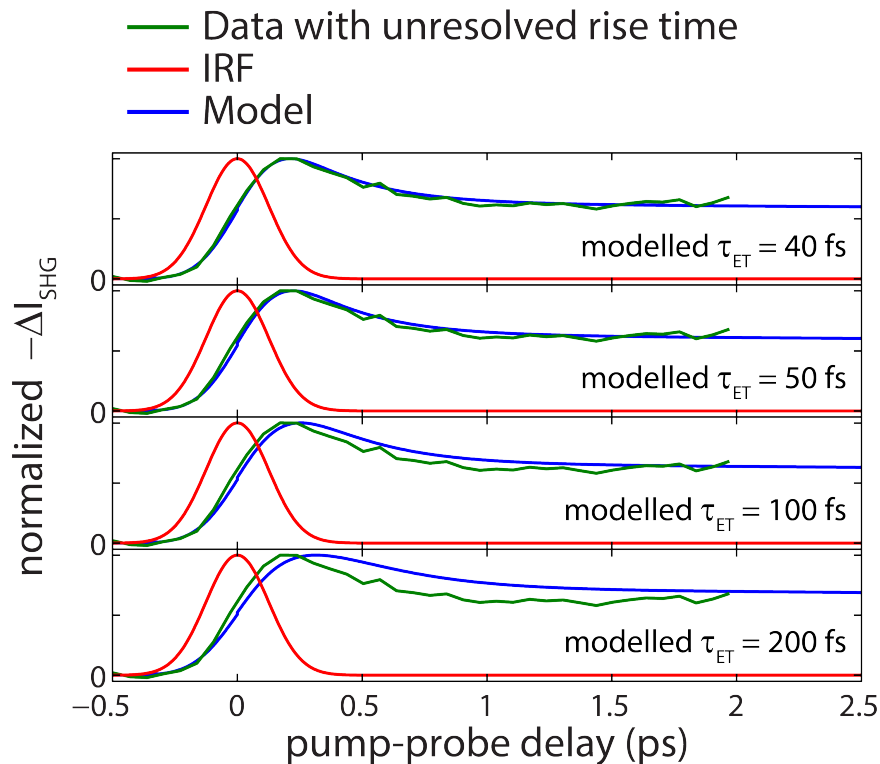


Figure 6: *Determining the minimum resolvable electron transfer time.* Transient SHG signal for ethane-thiol coated dots is plotted in green. The electron transfer time for this data is not resolvable by our measurement and the rise time represents the width of the IRF (plotted in red). Blue lines represent fits to the data in green with altered input values for the electron transfer rate constant k_{ET} .

Table of Fitted Parameters

Below is a table of best fit parameters for the transient curve fitting described above.

Ligand	Observed Values (s⁻¹)	Average Value (s⁻¹)
ethane-thiol		
k_{ET}	(>2e13, >2e13, >2e13)	>2e13
k_{decay} , fixed across samples		1e12
k_{diff1}	(2e12, 1e13, 5e12)	5e12
k_{diff2}	(2e10, 1e10, 1e10)	1e10
k_{cool} , fixed across samples		1.4e12
butane-thiol		
k_{ET}	(>2e13, >2e13)	>2e13
k_{decay} , fixed across samples		1e12
k_{diff1}	(6.7e11, 1e12)	8e11
k_{diff2}	(2e10, 3e11)	2e11
k_{cool} , fixed across samples		1.4e12
octane-thiol		
k_{ET}	(>2e13, 2.7e12, 7.1e12)	1.0e13
k_{decay} , fixed across samples		1e12
k_{diff1}	(1e10, 1e10, 1e10)	1e10
k_{diff2}	(5e11, 2e10, 5e10)	2e11
k_{cool} , fixed across samples		1.4e12
dodecane-thiol		
k_{ET}	(1.4e12, 1e13, >2e13)	1.0e13
k_{decay} , fixed across samples		1e12
k_{diff1}	(1e10, 2e12, 8e11)	9e11
k_{diff2}	(1e10, 1e10, 1e10)	1e10
k_{cool} , fixed across samples		1.4e12

Experimental Details

Optical Setup

For the transient SHG experiment, the light source was a 76 MHz Ti:sapphire oscillator (Coherent, Mira-HP) generating 100 fs, $\lambda = 830$ nm pulses. The oscillator synchronously pumps an optical parametric oscillator (OPO, Coherent, Mira-OPO). The OPO generated 100 fs pulses of tunable wavelength ($\lambda = 550$ to 700 nm). Pulses in the pump beam were temporally compressed using a pair of dispersive prisms (Thorlabs, AFS-SF10). The pump power at the sample was controlled using a gradient neutral density filter wheel (Thorlabs, NDC-50C-2M). The pump-probe delay was controlled by directing the pump beam into a retroreflector mounted on a precision delay stage (Thorlabs, DDS220). To isolate the pump-induced change in the SHG signal, the pump beam was mechanically chopped at 5 kHz (Thorlabs, MC2000B). Before entering the microscope, the pump beam was expanded, collimated, and spatially filtered using a pinhole confocal with two aspheric lenses (Thorlabs, molded glass asphere: $f = 5$ mm, AC254-030-A: $f = 30$ mm). The pump beam was then combined with the probe beam using a 50:50 beam splitter. The pump fluence at the sample is characterized by the following parameters: fluence = 0.15 mJ/cm² per pulse, pulse energy = 1.2 nJ, spot radius = 0.5 μ m, repetition rate = 76 MHz.

The probe beam was picked off from the Mira output prior to the OPO and temporally compressed using a dispersive prism pair before being similarly expanded, collimated, and spatially filtered. The probe was then combined with the pump beam using a 50:50 beam splitter. Both beams were then aligned into an inverted microscope (Nikon Ti-U) and reflected into the microscope objective (Nikon, CFI S Plan Fluor ELWD, 40 \times , 0.6 numerical aperture) using a 50:50 beam splitter. The probe fluence at the sample is characterized by the following parameters: fluence = 2.0 mJ/cm² per pulse, pulse energy = 16 nJ, spot radius = 0.5 μ m, repetition rate = 76 MHz. The back-propagating SHG radiated from the atomically thin sample was captured with the same objective, and the fraction passed by

the beam splitter was filtered (Thorlabs, FES0450 and FGB39; Semrock, FF01-440/SP-25) and detected by a photomultiplier tube (see below).

The WS_2/QD sample was susceptible to photoinduced degradation in air. To prevent this, all data were collected with the sample under vacuum ($< 10^{-4}$ Torr). This was achieved by measuring the sample in an evacuated cryostat (Janis Research, ST-500 microscopy cryostat) at room temperature.

Detection Electronics

SHG photons were detected by a photomultiplier tube (Hamamatsu, R4220P) biased at 1250 V using a high voltage power supply (Stanford Research Systems, PS325). The current pulses generated by the photomultiplier tube were analyzed using a gated photon counter (Stanford Research Systems, SR400) with the discriminator set to -0.03 V

Data Acquisition

The gated photon counter was triggered off of the reference signal generated by the mechanical chopper (5 kHz) in the pump beam. The counter recorded detection events for two 100 μs windows during each chopping period: one window recorded SHG counts while the pump was blocked and one window recorded counts while the pump was unblocked. The total number of counts in the absence of a pump represented the baseline SHG signal; the difference in the number of SHG counts when the pump was blocked and unblocked represented the pump-induced change in the SHG signal. The transient signal $-\Delta I_{\text{SHG}}/I_{\text{SHG}}^0$ represents the ratio of these two numbers and was negative in these experiments representing a pump-induced decrease in the SHG signal as discussed in the main text.

To collect a transient SHG trace the delay stage was scanned over a predetermined set of delay times. After the delay stage stabilized at each point, the transient SHG signal was collected for 1 s before moving to the next point. After all of the points were measured, the scan was repeated until adequate signal was collected. The data in Fig. 4 in the main text

contain 200 points and represent the average of roughly 70 scans. For perspective, these scans represent 4 hours of data acquisition and took roughly 5 hours in real time (due to the time needed to move the delay stage). Oftentimes instability in the experiment (e.g. microscope drift) limited the length of time for which data could be acquired; the experiment is highly sensitive to both the sample lateral position and focus.

WS₂ Exfoliation

WS₂ monolayers were mechanically exfoliated from a bulk single crystal (2D Semiconductors) on a Si/SiO₂ substrate. Adhesive tape (Ultron Systems, 1007R-6.0) was used to exfoliate WS₂. A piece of tape was lightly touched to the single crystal to pick up material. A second piece of tape was then laid flat onto the first and the two were firmly pressed together. The two pieces of tape were then slowly separated while maintaining a small angle ($< 30^\circ$) between the two pieces of tape. This procedure was then repeated 3-4 more times by placing a new piece of tape onto the most recently exfoliated piece of tape and before pulling the two apart. The final piece of tape held many WS₂ flakes ranging in thickness from a monolayer (rare) to quite thick. This piece of tape was laid flat on the Si/SiO₂ substrate. The WS₂ flakes were transferred to the substrate by vigorously rubbing the surface of the tape with a piece of rigid cardboard for 5 minutes. The tape was then slowly (~ 5 minutes) removed from the substrate by hanging a light weight from the tape's end allowing gravity to apply a constant force.

WS₂ monolayer flakes were then identified in the optical microscope by their bright photoluminescence. Monolayers were found by scanning the sample under UV illumination and looking for the (filtered) orange luminescence easily visible by eye characteristic of a monolayer. Once located, individual monolayer flakes and surrounding area were catalogued with photoluminescence images and optical micrographs. This allowed for the quick retrieval and recall of unique monolayer flakes (even after QD deposition). After deposition, the same catalogued flakes were found. The laser was aligned with the monolayers using the similarity

of the WS_2 flake arrangement before and after QD deposition. The presence of the WS_2 monolayers were further corroborated by the uniquely large SHG signal they produced. This is necessary because the WS_2 PL is substantially obscured by the presence of the QDs.

The QD deposition procedure described in the main text results in a multilayer of QDs that varies in thickness across the sample. The morphology of the QD film is illustrated in the SEM image in Fig. 7. Though there are many QD multilayers, QDs that are not in direct contact with the surface are unlikely to contribute to the pump-induced transient SHG signal, because they are not strongly electronically coupled with the WS_2 .

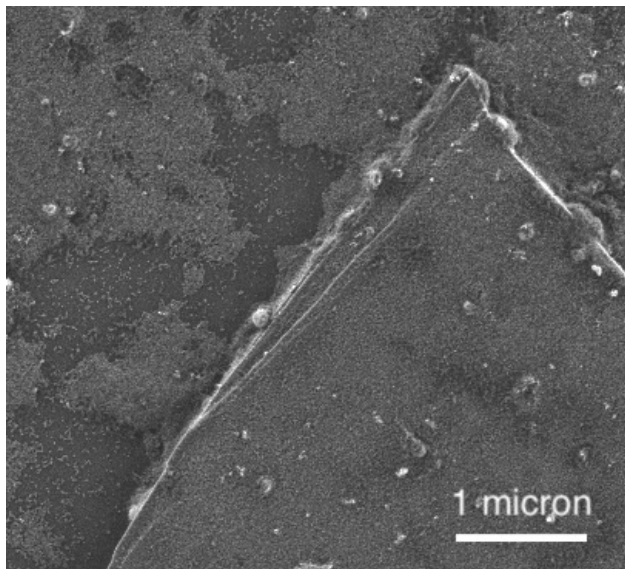


Figure 7: SEM image showing the typical morphology of a spun-cast QD film on a thick WS_2 flake. The QD film is not homogeneous but exhibits good coverage.